The Balmer Decrement of T Coronae Borealis from a Large and Heterogeneous Sample of Spectra

Kenneth Carrell
Angelo State University, 2601 W. Avenue N, San Angelo, TX 76909; kenneth.carrell@angelo.edu; ORCID: 0000-0002-6307-992X

Kennedi A. Walls
O'Fallon Township High School, O'Fallon, IL; kennedia.walls@gmail.com

Ronald Wilhelm
University of Kentucky, Lexington, KY; ron.wilhelm@uky.edu; ORCID: 0000-0002-4792-7722

James R. Foster
Pinon Pines RoR Observatory, Frazier Park, CA

David Cejudo
Observatorio El Gallinero, El Berrueco, Spain

Received February 2, 2026; revised June 15, 2026; accepted June 22, 2026

Abstract The Balmer decrement is an important probe of the physical conditions of gas and dust. This measurement will be a critical tool to describe the reddening and attenuation before, during, and after the eruption of T CrB. We show that the Balmer decrement can be measured using equivalent widths from a large heterogeneous sample of spectra. Being able to extract meaningful science results from samples such as this will allow us to leverage the tremendous amount of data, effort, and time spent by observers all around the world who will document the eruption of T CrB in more detail than any other nova eruption in history.

1. Introduction

Because of its anticipated imminent eruption (Schaefer 2023), the recurrent nova T CrB will likely be the most studied eruption in history. In fact, many professional and amateur astronomers alike have been monitoring this binary for many years now; the American Association of Variable Star Observers International Database (AAVSO) has almost 700,000 photometric observations of T CrB from 1995 until the end of July 2025 (AAVSO 1995–2025). The pre-eruption data will be an important baseline for comparison in the days, weeks, months, and years following the eruption itself.

There are many physical properties of the binary system that need to be understood to give a more complete picture of the eruption and its components. A critical aspect will be physical conditions of the gas and dust in and around the binary. An important probe of this is the Balmer decrement, the use of which dates back almost a century now (see, e.g. Berman 1936; Menzel and Baker 1937; Baker and Menzel 1938). Recently, Maslennikova *et al.* (2023) obtained flux calibrated spectra of T CrB between early-2020 and mid-2023 and were able to determine the Balmer decrement during this time. While results from coordinated, homogeneous samples such as this will be important, it will also be necessary to obtain results from observations using a wide variety of optical systems and instruments. Therefore, we have employed a method using equivalent widths (EWs) of the Hα and Hβ emission lines to determine the Balmer decrement for a much larger and much more heterogeneous spectroscopic sample.

In the following, we will discuss our data sample, an analysis of the velocities obtained from the spectra, and our determination of the Balmer decrement for T CrB. We end with a description of our results and conclusions.

2. Data

Spectroscopic observations for analysis were obtained from two sources: the AVSpec database hosted by AAVSO (Kloppenborg 2019–2025), and the Astronomical Ring for Amateur Spectroscopy (ARAS) Spectral Database (Teyssier 2019). The AVSpec database has spectra of T CrB dating back to early 2019, and we downloaded all data up to and including July 31, 2025 which gave us 657 individual spectra. The ARAS database for T CrB extends back to 2012, and downloading all spectra up to and including July 31, 2025 gave a total of 498 individual spectra. Because of a small number of overlapping spectra between the databases, and a few having issues with header values in the FITS files, in the end we had 1,131 unique spectra to analyze. Table A1 in Appendix A lists the observer codes and number of spectra contributed to our sample from both the AVSpec and ARAS databases. Of the spectra that had a resolution header keyword, most had a reported R between about 400 and 1,000, however there were also a number of spectra with R between about 10,000 and 15,000.

3. Analysis

The spectroscopic sample was extremely heterogeneous; it had a wide range of resolutions, wavelength coverage, and calibration status. This required a robust analysis procedure that could handle, and not be affected by, any of these differences.

3.1. Velocities

As has been previously reported (see, e.g., Stanishev *et al.* 2004; Zamanov *et al.* 2005; Munari 2023; Planquart *et al.* 2025), the Balmer emission lines do not follow the radial velocity of either the red giant (RG) or white dwarf (WD) component of the binary, and the emission lines can be quite complex with multiple emission peaks in addition to absorption features overlaid. However, as an initial check of both the data and analysis quality, we determined a radial velocity for both Hα and Hβ in each file (if present). This allowed us to see if both emission features have similar contributions from the various parts of the binary system. Rather than trying to fit a complex line profile, we instead computed a simple weighted mean from the normalized spectra in the range of ±10 Å from the center of mass rest wavelength for each line. When we restrict our original sample to unique entries that have enough header information to determine a heliocentric correction for the velocity, we end up with 867 spectra with an Hα and/or Hβ line. The velocity trends, along with a modeled radial velocity curve (Fekel *et al.* 2000) can be found in Figure 1. In these plots, the individual measurements can be seen as well as binned averages with standard error overlaid (bins are 5% of the phase). For phases of 1.0–2.0 the binned data and model radial velocity are repeated for clarity. These plots suggest that during the most recent active phase, the radial velocity of the Balmer emission lines do not strongly follow either of the binary components (there is a slightly better agreement with the WD component, although it is not very strong). However, during the recent quiescent phase, the velocity does follow the WD component much more closely, especially at phases > 0.5. We should note that the recent quiescent phase is only approximately one complete orbital cycle, which may cause the disagreement for smaller phases. The velocity information shows that there are definite differences in the spectra during the active and quiescent phases, which is to be expected. It also shows that there is not an obvious systematic difference between the overall profiles of the Hα and Hβ lines in either case.

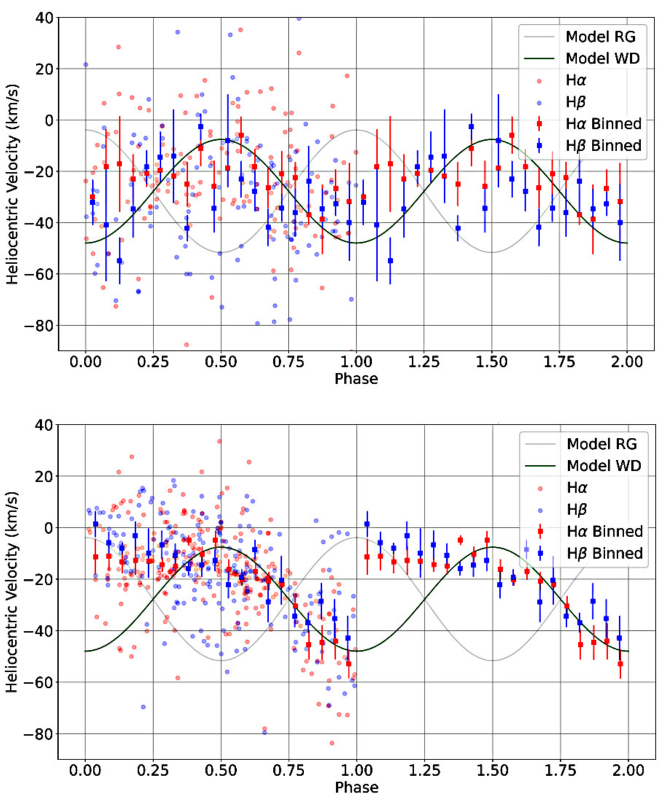

Figure 1. Heliocentric velocity as a function of orbital phase of the Hα and Hβ emission lines calculated from a weighted average of the normalized spectra. Observation dates are restricted to a recent active phase of T CrB (upper plot, 2457000 < HJD < 2460000) and a recent quiescent phase (lower plot, HJD > 2460650).

3.2. The Balmer decrement

As mentioned above, we do not know the exact status of the reduction of all of the spectra. Some have been flux calibrated, while others have only been wavelength calibrated. Because of this heterogeneity, we cannot determine the Balmer decrement using the flux in the spectra. Instead, we used Equation 2 of

$$\log(\mathrm{H}/\mathrm{H}\beta) = \log\left(\frac{\mathrm{EW}(\mathrm{H}\alpha)+3.5}{\mathrm{EW}(\mathrm{H}\beta)+3.5}\right) + [-0.26 + 0.39(g-r)] \quad (1)$$

Groves *et al.* (2012) to calculate the Balmer decrement from the EW of the Hα and Hβ lines in each of the spectra:

We have used the smaller correction for stellar absorption of 3.5 as recommended by Groves *et al.* (2012) for emission lines with smaller EWs. The photometric values of g = 10.891 and r = 9.718 were taken from Abazajian *et al.* (2009). We note, however, that while the photometry has flags indicating it may have errors, and subsequent data releases from the Sloan Digital Sky Survey have slightly varying values for both g and r, this color term is a small constant added to the ratio of the EWs and does not significantly alter our results or conclusions.

There are periodic changes in magnitude for the T CrB system both from an orbital and activity standpoint. Additionally, different bandpasses change by different amounts. Therefore, one could use archival photometry to determine a (g–r) color for the time each of the individual spectra were taken. However, most archival photometry, especially in the AAVSO database, are in the Johnson-Cousins photometric system. There are transformation equations to convert from the $UBVR_cI_c$ system to the ugriz system (e.g. Jester *et al.* 2005), but these are often for very specific sets of objects, e.g. quasars at $z \leq 2.1$, or stars with $R_c–I_c < 1.15$ and U–B < 0. Since T CrB does not fall into any of the typical categories for transformation, choosing one over another would be difficult and could introduce errors. Furthermore, the (g–r) term in the equation above is used as a proxy for the stellar continuum. Color changes for T CrB are not due to changes in the stellar component continuum itself, but from differing contributions of the hot component (accretion disk) and different viewing angles of the binary system. Therefore, if we use archival B photometry, which has a large change during active phases of the binary because of increased light output from the accretion disk, we would derive (g–r) colors that do not accurately represent the stellar continuum in the Hα and Hβ regions of the spectra, introducing an error in our Balmer decrement values. As a result, we have used a constant (g–r) value in our calculations.

Since we did not know if the spectra were flux calibrated or normalized, we performed our own normalization on each one. We used the wavelength regions of 6525–6535 Å and 6590–6600 Å to determine the continuum level of the Hα emission feature, and 4825–4835 Å and 4885–4895 Å for Hβ. We fit the regions for each emission feature with a straight line, and normalized the spectrum in that area with the fitted function. Because of the complicated nature of the Balmer emission lines, including different radial velocity components, one cannot define a specific region for determining the EW for all spectra. Instead, we dynamically determine the best width for each individual spectrum. We first find the maximum flux in the region and use that as a central value. Starting with a window width of 5 Å and going up to 50 Å in steps of 5 Å, we determine the EW. Once the entire Balmer feature is within the window, an increase in the window size does not significantly change the EW. We select the best EW value by finding two consecutive window sizes with a difference of less than 1% in their EWs. By dynamically determining the best window, we can accommodate spectra with widely varying resolutions and emission features.

4. Results

In Figure 2 we show the EW of both the Hα and Hβ emission lines for the entire sample. One can see the two follow each other and are offset from one another.

We determine the Balmer decrement using two techniques. For spectra that have both the Hα and Hβ lines present, we use those EWs to determine the Balmer decrement, resulting in a measurement from homogeneous data. This broad spectral coverage is only typical for the low-resolution spectra— higher resolution spectra typically covers only Hα or Hβ but not both. We take all the spectra with only a single line present and match them in time to the closest measurement of the other line, requiring the time difference to be less than 8 hours, which ensures the spectra are taken relatively close in time (within the same night). So, an individual Hα line gets matched to the individual Hβ line closest in time, and vice versa. The Balmer decrement for the full sample is shown in Figure 3. Data before 2017 are rather sparse, but from 2017 until 2023, during an active state for the binary, the Balmer decrement of T CrB remained relatively constant between about 3 and 4. Since 2023, however, T CrB has returned to a more quiescent state and has had much larger variations in the Balmer decrement. Data for 2025 (during a quiescent phase) can be seen in Figure 4 to have a definite structure.

Most of the single-line (i.e. higher resolution) data have been taken more recently in time, so in Figure 4 we compare the Balmer decrement determined from a single spectrum to those from different spectra. The values determined from a single spectrum come from more homogeneous data, and the matched values come primarily from higher resolution observations. As can be seen in Figure 4, the results from each sample agree very well, which gives us confidence that this method of determining the Balmer decrement gives robust results that are not heavily dependent on spectral resolution.

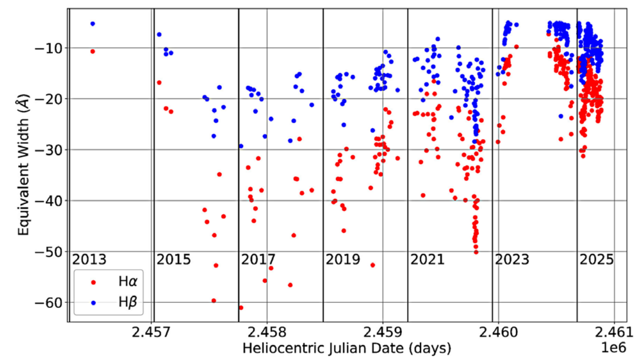

Figure 2. Equivalent widths of the Hα and Hβ emission lines for our entire sample of T CrB spectra. The horizontal axis is the Julian date, and vertical lines are the first day of the labeled calendar year.

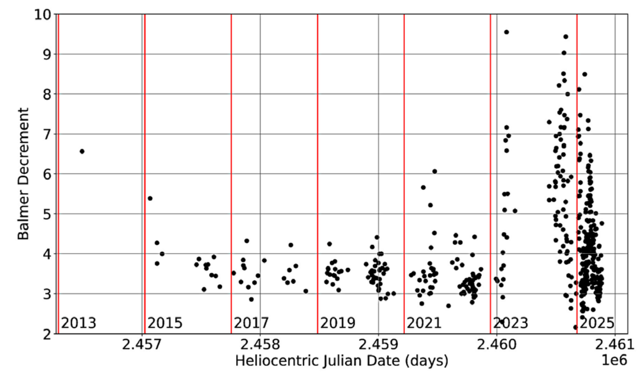

Figure 3. The Balmer decrement of T CrB from our entire sample. As in Figure 2, the vertical lines mark the beginning of the labeled calendar years.

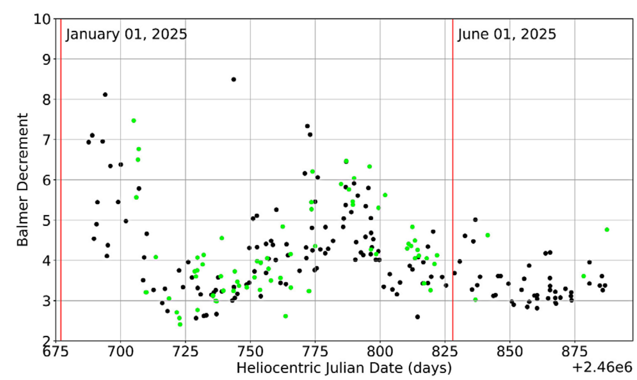

Figure 4. The Balmer decrement of T CrB for approximately the first half of 2025. Black points are values determined from a single spectrum and green points are determined by combining results from two different spectra (one each for Hα and Hβ).

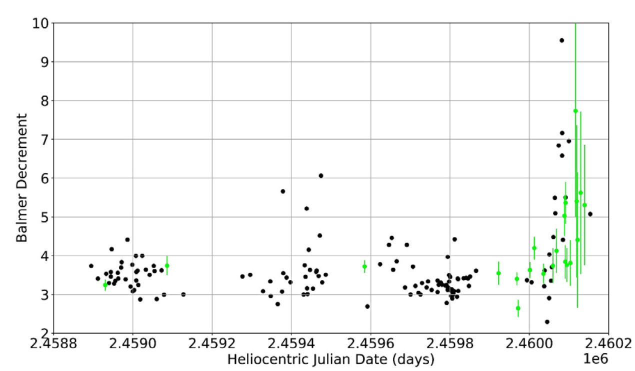

Figure 5. The Balmer decrement of T CrB from our results (black points) and those from Maslennikova *et al.* (2023) (green points with errorbars).

Maslennikova *et al.* (2023) were able to measure the Balmer decrement of T CrB from early-2020 to mid-2023 using flux calibrated spectra. Their Figure 11 shows their results: from their first measurements in 2020 until mid-2023 the Balmer decrement stays between ~3–4. In mid-2023 (a Julian date of about 2460100) the values rise quickly, with many between 5 and 10. In Figure 5 we plot the results from Maslennikova *et al.* (2023) along with our results from the same time period. One can see that our Balmer decrement agrees very well with those determined from actual flux measurements of flux calibrated spectra of T CrB. This again gives us confidence in our method.

5. Conclusions

The Balmer decrement is an important tool to probe properties of the T CrB system. It can show the amount of extinction and dust obscuration because of the depth dependence of the optical depth, but it can also indicate changes in the UV and X-ray continuum (see e.g. Maslennikova *et al.* 2023; Wu *et al.* 2023; Gaskell and Ferland 1984, and references therein). Although the Balmer decrement is typically determined from a homogeneous sample of flux calibrated spectra (e.g. Maslennikova *et al.* 2023), we have shown that we can recover useful results from large data sets of very heterogeneous data that agree with those from homogeneous samples. Extracting meaningful results from data sets such as this will allow for more science to be done when the unpredictable eruption does occur, and allows for a much larger community to contribute to the scientific process.

6. Acknowledgements

For their time and effort, we would like to thank the observers who submitted spectra to the AAVSO and ARAS databases that were used in this work. These observers are listed in Table A1.

We wish to thank N. A. Maslennikova for providing the data used to produce a figure in their published work that is represented in our Figure 5.

We wish to thank the anonymous referee for providing feedback that improved the quality of this work.

Facilities: AAVSO, ARAS

References

AAVSO. 1995–2025, variable star observations from the AAVSO International Database (https://apps.aavso.org/v2/data/search/photometry/).

Abazajian, K. N., *et al.* 2009, *Astrophys. J., Suppl. Ser.*, **182**, 543 (DOI: 10.1088/0067-0049/182/2/543).

Baker, J. G., and Menzel, D. H. 1938, *Astrophys. J.*, **88**, 52 (DOI: 10.1086/143959).

Berman, L. 1936, *Mon. Not. Roy. Astron. Soc.*, **96**, 890 (DOI: 10.1093/mnras/96.9.890).

Fekel, F. C., Joyce, R. R., Hinkle, K. H., and Skrutskie, M. F. 2000, *Astron. J.*, **119**, 1375 (DOI: 10.1086/301260).

Gaskell, C. M., and Ferland, G. J. 1984, *Publ. Astron. Soc. Pacific*, **96**, 393 (DOI: 10.1086/131352).

Groves, B., Brinchmann, J., and Walcher, C. J. 2012, *Mon. Not. Roy. Astron. Soc.*, **419**, 1402 (DOI: 10.1111/j.1365-2966.2011.19796.x).

Jester, S., *et al.* 2005, *Astron. J.*, **130**, 873 (DOI: 10.1086/432466).

Kloppenborg, B. 2019–2025, AVSpec, variable star observations from the AAVSO Spectral Database (https://apps.aavso.org/avspec/search).

Maslennikova, N. A., Tatarnikov, A. M., Tatarnikova, A. A., Dodin, A. V., Shenavrin, V. I., Burlak, M. A., Zheltoukhov, S. G., and Strakhov, I. A. 2023, *Astron. Lett.*, **49**, 501 (DOI: 10.1134/S1063773723090037).

Menzel, D. H., and Baker, J. G. 1937, *Astrophys. J.*, **86**, 70 (DOI: 10.1086/143844).

Munari, U. 2023, *Res. Notes Amer. Astron. Soc.*, **7**, 251 (DOI: 10.3847/2515-5172/ad0f26).

Planquart, L., Jorissen, A., and Van Winckel, H. 2025, *Astron. Astrophys.*, **694A**, 85 (DOI: 10.1051/0004-6361/202452833).

Schaefer, B. E. 2023, *Mon. Not. Roy. Astron. Soc.*, **524**, 3146 (DOI: 10.1093/mnras/stad735).

Stanishev, V., Zamanov, R., Tomov, N., and Marziani, P. 2004, *Astron. Astrophys.*, **415**, 609 (DOI: 10.1051/0004-6361:20034623).

Teyssier, F. 2019, *Contrib. Astron. Obs. Skalnate Pleso*, **49**, 217.

Wu, J., Wu, Q., Xue, H., Lei, W., and Lyu, B. 2023, *Astrophys. J.*, **950**, 106 (DOI: 10.3847/1538-4357/acce9e).

Zamanov, R., Gomboc, A., Bode, M. F., Porter, J. M., and Tomov, N. A. 2005, *Publ. Astron. Soc. Pacific*, **117**, 268 (DOI: 10.1086/428069).

Appendix A: Observers

Table A1 provides a list of all observer codes and the number of spectra contributed that were used in the analysis. There was some overlap in observers between the two databases and where possible they were combined into the AAVSO table.

Table A1. Table of the number of observations from AAVSO and ARAS contributors.

AAVSO

AAVSO Observer Code	*Observer*	*Number of Spectra*	*AAVSO Observer Code*	*Observer*	*Number of Spectra*
FJQ	James R. Foster	368	TSHB	Shuichi Tsuda	4
CDZ	David Cejudo	104	HJOI	Joe Hobart	3
SKEC	Keith Shank	60	BGAK	Gary Bertollini	2
GKEA	Kevin N. Gurney	26	DMAD	Massimo Di Lazzaro	2
TDW	David Trowbridge	20	MBM	Associazione Astrofili Fiorentini	2
MDJ	Daniel Jose Mendicini	15	RGN	Gianluca Rossi	2
DDGB	Dave G. Decker	13	CJOH	Johannes D. Clausen	1
GSTD	Stefan Güssregen	10	FPAB	Patrick Fricker	1
DJED	Jean-Bruno Desrosiers	9	IDG	David Iadevaia	1
DSN	Scott Donnell	9	LJOJ	Jonathan Lachapelle	1
LMN	Magnus Larsson	9	MMOI	Tec Moises Montero	1
PROI	Rosario Pomillo	9	SPHE	Philipp Stiegler	1
ERAA	Ing Rainer Ehlert	7	STIB	Tim Stone	1
BHU	Robert Buchheim	6	WME	Myron E. Wasiuta	1
FLOA	Lorenzo Franco	4			

ARAS

ARAS Observer Code	*Observer*	*Number of Spectra*	*ARAS Observer Code*	*Observer*	*Number of Spectra*
JRF	J. Foster	100	GBE	G. Bertrand	2
FAS	F. Sims	42	SOL	U. Sollecchia	2
XDU	X. Dupont	37	VBO	V. Bouttard	2
CBO	C. Boussin	24	CEL	C. Eldridge	1
PAD	P. Dubovský	23	GKA	K. Graham	1
DBO	D. Boyd	21	GMYB	G. Martineau and Y. Buchet	1
EBE	E. Bertrand	20	HBO	H. Boussier	1
FTE	F. Teyssier	20	JBD	J. Desrosiers	1
PSO	P. Somogyi	20	JCO	J. Coffin	1
JGF	J. Flo	19	JLE	J. Lecomte	1
RLE	R. Leadbeater	19	JMI	J. Michelet	1
ALE	A. Leduc	11	JMO	J. Montier	1
CLC	C. Laulhère	10	JPM	J. Masviel	1
IBR	I. Diarrassouba	10	LES	T. Lester	1
SARO	R. Pomillo	8	MPI	M. Pilisi	1
CUR	S. Curry	6	MRO	M. Rodrigues	1
JDH	J. Lemaire	5	OGA	O. Garde	1
FCP	F. Campos	4	PLO	P. Louis	1
FRA	L. Franco	4	SCH	S. Charbonnel	1
VLE	V. Lecoq	4	TME	T. Medulka	1
BUI	C. Buil	3	TRO	T. Rodda	1
KGU	K. Gurney	3	YMA	Y. Markus	1
FBO	F. Boubault	2			